J. Fluid Mech. (1990), *vol.* 216, *pp.* 231–254
Printed in Great Britain

The axisymmetric deformation of a red blood cell in uniaxial straining Stokes flow

By C. POZRIKIDIS

Department of Applied Mechanics and Engineering Sciences, R-011, University of California, San Diego, California 92093, USA

(Received 5 May 1989)

The axisymmetric deformation of a red blood cell placed in a uniaxial straining Stokes flow is considered. The cell is modelled as a fluid capsule that contains a Newtonian fluid, and is bounded by an area-preserving membrane with negligible resistance to bending. First, it is theoretically demonstrated that spheroidal cells with isotropic membrane tension constitute stationary configurations. To compute transient cell deformations, a numerical procedure is developed based on the boundary-integral method for Stokes flow. Calculations show that initially prolate or oblate cells with isotropic membrane tension deform into stationary spheroids. Cells with a highly oblate initial shape may develop a persistent small pocket along their axis during the deformation. The shear elasticity of the membrane prevents folding, but may cause the formation of sharp corners and concave regions along the cell contour. A decrease in the membrane shear elasticity results in substantial increase in the magnitude of the transient and asymptotic membrane tensions. The maximum strain rate below which a red blood cell remains intact is estimated to be $e_{\max} = 10^5\ \mathrm{s}^{-1}$.

1. Introduction

Red blood cells are fluid capsules that contain a nearly Newtonian solution of haemoglobin and are bounded by a flexible biological membrane (Evans & Skalak 1980). Under normal quiescent conditions, the red blood cells assume the shape of biconcave disks, that is, disks with a double-sided dimple at the centre. The large diameter of a red blood cell is approximately equal to 8 μm. The unstressed cell shape may be modified by altering the tonicity of the suspending fluid. The cell membrane consists of a mobile double molecular layer of lipids and several proteins which is supported by a rigid network of a protein called spectrin. This rather complex structure renders the cell membrane an area-preserving (incompressible), two-dimensional medium with small resistance to shearing deformation, and extremely small resistance to bending. The mammalian red cell is the only biological cell known to have a structureless, liquid interior and an area-preserving membrane.

When a red blood cell is placed in a straining flow, it starts deforming much like a liquid droplet. When the straining flow is rotational and the shear rate is above a threshold value, the cell membrane deforms as well as rotates in a 'tank-treading' mode, inducing internal circulation (Keller & Skalak 1982). Unlike a liquid drop, a red blood cell may not deform without limit owing to the virtually constant area of the bounding membrane. As the intensity of the imposed straining flow is increased the membrane tension escalates to higher levels, eventually leading to rupture and hemolysis. Understanding how a red blood cell deforms and breaks up under the

action of the straining flow is a problem of fundamental medical significance. First, it provides information on the instantaneous cell shape and membrane tension during large-scaled blood flow. Second, it supplies us with useful guidelines for the design of artificial circulation organs such as cardiac valves. Furthermore, as noted by Fung (1981), the study of red blood cell deformability is of clinical value, for changes in shape, size, and strength of red cells may be indicative of a blood disease (for a particular example see Fischer 1989).

Ideally, one would like to tackle the problem of red-cell deformation in its exact formulation, coupling the external to the internal cell flow, and taking into consideration the exact mechanical characteristics of the cell membrane. This turns out to be a difficult task, calling for simplifying assumptions in regard to the unstressed cell shape, the cell membrane mechanical characteristics, or both. In this spirit, Barthes-Biesel (1980), Barthes-Biesel & Rallison (1981), Li, Barthes-Biesel & Helmy (1988) and Brunn (1983) considered small transient deformations of a nearly spherical capsule which is imbedded in shear flow. Li *et al.* (1988) considered the axisymmetric deformation of a cell placed in uniaxial straining flow assuming that the cell membrane exhibits elastic behaviour and relaxing the condition of incompressibility. Keller & Skalak (1982) considered non-deforming ellipsoidal cells, where the cell membrane moves with a prescribed velocity, with interest in capturing the main effects of the membrane tank-treading motion. A number of other authors have presented two-dimensional models for infinite flow or for flow within confined channels (Niimi & Sugihara 1985; Zahalak, Rao & Sutera 1987).

In the present work we study the deformation of a cell in an imposed uniaxial straining flow. In our analysis, we consider unstressed cell shapes that resemble those of red blood cells, and use an accurate model for the mechanical response of the cell membrane. Specifically, we assume that the membrane is a two-dimensional area-preserving (incompressible) medium with finite shear elasticity but negligible resistance to bending (Skalak, Oskaya & Skalak 1989). The most critical approximation in our analysis is the assumption of axisymmetric deformation, adopted purely for analytical and computational convenience. Admittedly, considering axisymmetric deformations prevents the membrane tank-treading motion, a feature that requires a genuinely three-dimensional deformation. A second assumption in our analysis is that the viscosity of the fluid within the cell is equal to that of the surrounding fluid. For a human red cell *in vivo*, the ratio between the viscosity of the internal and external fluid is approximately equal to five. In experimental flows, however, this ratio is readily controlled, and it is usually set to a value less than one (Tran-Son-Tay, Sutera & Rao 1984).

To make our investigation more comprehensive, we examine cells with a variety of unstressed shapes including oblate and prolate spheroids. Our objectives are to document the possible modes of cell deformation, to assess the significance of membrane shear elasticity, and to compute the magnitude of the membrane tensions developing during the cell deformation. Our analysis proceeds in two stages. First, we study a family of stationary cells with isotropic membrane tension that are imbedded in a uniaxial straining flow. These are viewed as asymptotic states of cells that have undergone a transient deformation. In the second stage we study transient cell deformations. For this purpose, we develop a numerical procedure which is based on the boundary-integral representation of Stokes flow (Rallison & Acrivos 1978). We thus represent the velocity field inside and outside the cell in terms of a distribution of fundamental solutions to the Stokes equation over the cell surface. The density of

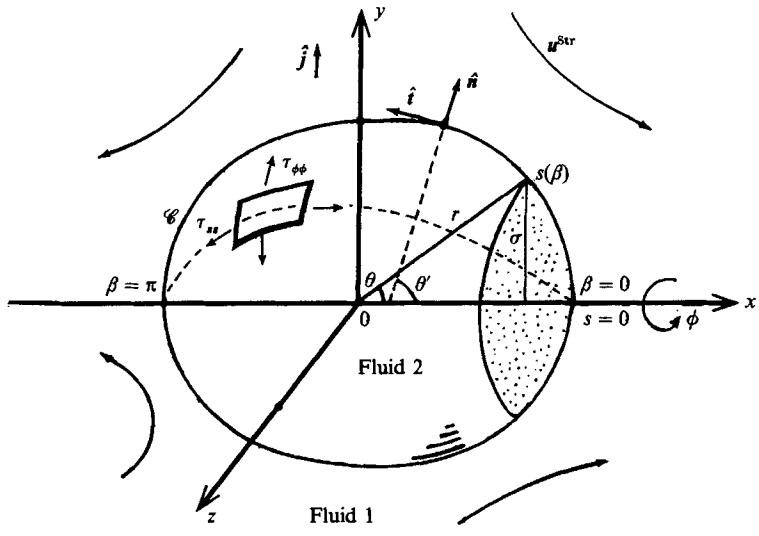

FIGURE 1. Schematic representation of an axisymmetric cell deforming in a straining flow; τ_{ss} and $\tau_{\phi\phi}$ are the meridional and azimuthal membrane tensions.

this distribution involves the principal membrane tensions. Combining this representation with a constitutive equation for the membrane stresses and with the condition of membrane incompressibility provides us with a linear integral equation for the principal membrane tensions. We solve this equation using a procedure that entails surface discretization and subsequent collocation. Overall, the numerical procedure of solution is similar to that employed in previous studies of drop or cell deformations, in particular those by Rallison & Acrivos (1978), Li *et al.* (1988), Pozrikidis (1990).

In §2 we formulate the problem as an integral equation, combining the equations of fluid flow inside and outside the cell with those of the mechanical equilibrium of the cell membrane. In §3 we show that spheroidal cells with isotropic membrane tension constitute stationary configurations. This renders the spheroidal shape a strong candidate for the asymptotic shape of a deformed cell. In §4 we present results of numerical computations for transient deformations, and in §5 we summarize and conclude our discussion.

2. Formulation

2.1. *The contour dynamics equation*

We consider the deformation of an axisymmetric cell which is imbedded in uniaxial straining flow at vanishing Reynolds number, as illustrated in figure 1. We denote the cell fluid with the index 2, and the suspending fluid with the index 1. In Cartesian coordinates with origin at the cell centre, the far-field flow is given by

$$\boldsymbol{u}^{\mathrm{Str}} = e \begin{bmatrix} 2 & 0 & 0 \\ 0 & -1 & 0 \\ 0 & 0 & -1 \end{bmatrix} \cdot \boldsymbol{x} \tag{2.1}$$

where e is the rate of strain. The cell contains a Newtonian fluid which is enclosed

by a thin biological membrane. The viscosity μ of the fluid inside the cell is assumed to be equal to the viscosity of the suspending fluid. At the outset we non-dimensionalize all variables using as a characteristic timescale $1/e$, lengthscale the equivalent cell radius $(3V/4\pi)^{\frac{1}{3}}$, stress scale μe, and tension scale $\mu e a$, where V is the cell volume. We then decompose the total flow into the far-field and disturbance components, where the latter is exclusively attributed to the presence of the cell. Using the boundary-integral formulation (Rallison & Acrivos 1978), we find that the total flow, both inside and outside the cell, may be expressed as

$$u_i(\boldsymbol{x}_0) = u_i^{\mathrm{Str}}(\boldsymbol{x}_0) - \frac{1}{8\pi}\int_{\mathrm{Cell}} \Delta f_j(\boldsymbol{x})\, S_{ji}(\boldsymbol{x}, \boldsymbol{x}_0)\, \mathrm{d}s(\boldsymbol{x}), \tag{2.2}$$

where $\Delta \boldsymbol{f}$ is the jump in surface stress across the surface of the cell defined by

$$\Delta \boldsymbol{f} = \boldsymbol{f}_1 - \boldsymbol{f}_2 = (\boldsymbol{\sigma}_1 - \boldsymbol{\sigma}_2)\cdot \hat{\boldsymbol{n}} \tag{2.3}$$

and $\boldsymbol{\sigma}$ is the stress tensor. The integral in (2.2) is over the surface of the cell, whereas the unit normal vector $\hat{\boldsymbol{n}}$ in (2.3) is directed *outside the cell* and into the ambient fluid, as indicated in figure 1. In (2.2), $\boldsymbol{S}$ is the free-space Stokeslet defined as

$$S_{ij}(\boldsymbol{x}, \boldsymbol{x}_0) = \frac{\delta_{ij}}{r} + \frac{\hat{x}_i \hat{x}_j}{r^3}, \tag{2.4}$$

where $\hat{\boldsymbol{x}} = \boldsymbol{x} - \boldsymbol{x}_0$, and $r = |\hat{\boldsymbol{x}}|$. If $\Delta \boldsymbol{f}$ is known, (2.2) may be used to compute the velocity at any point inside, outside, and more importantly, on the surface of the cell.

For axisymmetric flow, the azimuthal component of $\Delta \boldsymbol{f}$ is equal to zero. Referring to the polar cylindrical coordinates (x, σ, ϕ) of figure 1, we write $\Delta \boldsymbol{f} = (\Delta f_x, \Delta f_\sigma, 0)$, and express Δf_x, Δf_y, and Δf_z, in terms of Δf_x and Δf_σ. Substituting into (2.2) and performing the integration in the azimuthal direction we obtain

$$u_\alpha(\boldsymbol{x}_0) = u_\alpha^{\mathrm{Str}}(\boldsymbol{x}_0) - \frac{1}{8\pi}\int_{\mathscr{C}} M_{\alpha\beta}(\boldsymbol{x}, \boldsymbol{x}_0)\, \Delta f_\beta(\boldsymbol{x})\, \mathrm{d}s(\boldsymbol{x}) \tag{2.5}$$

where Greek indices take the value 1 or 2 for the x- and σ-direction respectively, and the integration is over the cell contour in a meridional plane, denoted by $\mathscr{C}$ in figure 1. In (2.5) $\boldsymbol{x} = (x, \sigma)$, and $\boldsymbol{x}_0 = (x_0, \sigma_0)$. The matrix $\boldsymbol{M}$ was given by Rallison & Acrivos (1978), but for completeness, it is also given in the Appendix. When the cell attains a stationary configuration, the velocity inside and on the surface of the cell is equal to zero, and the pressure inside the cell is constant.

2.2. *The mechanical behaviour of the membrane*

Before we can use (2.5) to compute the deformation of the cell, it is necessary to define the discontinuity in surface stress Δf_α, $\alpha = 1, 2$, taking into consideration the mechanical characteristics of the cell membrane. For this purpose, it is convenient to decompose $\Delta \boldsymbol{f}$ into its normal and tangential components

$$\Delta \boldsymbol{f} = (\Delta \boldsymbol{f}\cdot \hat{\boldsymbol{n}})\, \hat{\boldsymbol{n}} + (\Delta \boldsymbol{f}\cdot \hat{\boldsymbol{t}})\, \hat{\boldsymbol{t}}. \tag{2.6}$$

Now, in general, a cell membrane may support both shear and normal stresses, implying that both the tangential and the normal component may have finite values. For a membrane with only in-plane stresses and negligible resistance to bending, such as the membrane of a red blood cell, $\Delta \boldsymbol{f}$ may be expressed with respect to the principal tensions of the membrane in the meridional and azimuthal direction, τ_{ss}

and $\tau_{\phi\phi}$ respectively (figure 1). Specifically, the equations of mechanical equilibrium of a material element on the membrane require that

$$\Delta \boldsymbol{f}\cdot\hat{\boldsymbol{t}} = -\left[\frac{\mathrm{d}\tau_{ss}}{\mathrm{d}s}+\frac{1}{\sigma}\frac{\partial\sigma}{\partial s}(\tau_{ss}-\tau_{\phi\phi})\right], \tag{2.7a}$$

$$\Delta \boldsymbol{f}\cdot\hat{\boldsymbol{n}} = k_s\tau_{ss}+k_\phi\tau_{\phi\phi} \tag{2.7b}$$

(see for instance Evans & Skalak 1980, p. 58). Here, k_s and k_ϕ are the curvatures of the surface of the cell in the meridional and the azimuthal direction, defined as

$$k_s = \frac{\mathrm{d}\theta'}{\mathrm{d}s}, \quad k_\phi = \frac{\hat{n}_\sigma}{\sigma}, \tag{2.8}$$

s is the arclength measured along the contour $\mathscr{C}$, θ' is the angle formed by the normal to the cell contour and the x-axis, $\hat{n}_\sigma = \hat{\boldsymbol{n}}\cdot\hat{\boldsymbol{j}}$, and $\hat{\boldsymbol{j}}$ is the unit vector in the σ-direction (figure 1). The unit tangent vector $\hat{\boldsymbol{t}}$ in (2.7a) is oriented in the counterclockwise direction, as indicated in figure 1. Furthermore, we may express the principal tensions τ_{ss} and $\tau_{\phi\phi}$ in terms of their mean (isotropic) and deviatoric components,

$$\tau_{ss} = \tau^{\mathrm{m}}+\tau^{\mathrm{d}}, \quad \tau_{\phi\phi} = \tau^{\mathrm{m}}-\tau^{\mathrm{d}}, \tag{2.9a, b}$$

where

$$\tau^{\mathrm{m}} = \tfrac{1}{2}(\tau_{ss}+\tau_{\phi\phi}), \quad \tau^{\mathrm{d}} = \tfrac{1}{2}(\tau_{ss}-\tau_{\phi\phi}). \tag{2.9c, d}$$

Substituting (2.9a, b) into (2.7a, b) and subsequently into (2.6) we obtain

$$\Delta \boldsymbol{f} = [(k_s+k_\phi)\tau^{\mathrm{m}}+(k_s-k_\phi)\tau^{\mathrm{d}}]\hat{\boldsymbol{n}}-\left[\frac{\mathrm{d}\tau^{\mathrm{m}}}{\mathrm{d}s}+\frac{\mathrm{d}\tau^{\mathrm{d}}}{\mathrm{d}s}+\frac{2}{\sigma}\frac{\partial\sigma}{\partial s}\tau^{\mathrm{d}}\right]\hat{\boldsymbol{t}}. \tag{2.10}$$

It is instructive to note that in the case of a liquid drop the deviatoric component τ^{d} vanishes, whereas the mean membrane tension τ^{m} is equal to the surface tension γ.

We proceed now to derive constitutive relationships for the membrane tensions. One relationship comes from the requirement that the surface area of the membrane remains locally and globally constant in time. To quantify this requirement, we introduce the Lagrangian parameter $\beta(0<\beta<\pi)$ marking individual material elements on a meridional contour of the membrane, and view the position of an element a function of time t and β (figure 1). The area of the dotted axisymmetric section of the membrane indicated in figure 1 is equal to

$$A(\beta,t) = 2\pi\int_0^\beta \sigma\frac{\partial s}{\partial\beta'}\mathrm{d}\beta'. \tag{2.11}$$

At this point, it is convenient to introduce the principal extension ratios λ_s and λ_ϕ

$$\lambda_s = \frac{\left(\dfrac{\partial s}{\partial\beta}\right)_t}{\left(\dfrac{\partial s}{\partial\beta}\right)_{t=0}}, \quad \lambda_\phi = \frac{(\sigma)_t}{(\sigma)_{t=0}}, \tag{2.12a, b}$$

where the membrane is assumed to be unstressed at $t=0$. Note that at the initial instant $t=0$, or along the axis of symmetry, $\lambda_s=\lambda_\phi=1$. We then rewrite (2.11) in the equivalent form

$$A(\beta,t) = 2\pi\int_0^\beta\left(\sigma\frac{\partial s}{\partial\beta'}\right)_{t=0}\lambda_s\lambda_\phi\,\mathrm{d}\beta'. \tag{2.13}$$

It is clear that in order for the area of the membrane to remain locally constant in time,

$$\lambda_s \lambda_\phi = 1 \tag{2.14}$$

for any value of β. Differentiating this equation with respect to time keeping β constant, we derive the desired condition of area preservation:

$$\boldsymbol{u}\cdot\hat{\boldsymbol{j}} + \sigma\hat{\boldsymbol{t}}\cdot\frac{\partial \boldsymbol{u}}{\partial s} = 0. \tag{2.15}$$

Substituting (2.5) into (2.15) we finally obtain

$$u_2^{\mathrm{Str}} + \sigma_0 \hat{t}_\alpha \frac{\partial u_\alpha^{\mathrm{Str}}}{\partial s_0} - \frac{1}{8\pi}\int_{\mathrm{Cell}} \left[M_{2\beta} + \sigma_0 \hat{t}_\alpha(\boldsymbol{x}_0)\frac{\partial M_{\alpha\beta}}{\partial s_0}\right]\Delta f_\beta \,\mathrm{d}s = 0, \tag{2.16}$$

where all variables are written in cylindrical polar coordinates. This equation defines a kinematic constraint for the cell deformation, and plays the role of a constitutive equation for the membrane tension.

To complete the definition of our problem we need an additional scalar constitutive equation. For lack of a better alternative, we set the deviatoric component of the tension equal to that for an isotropic elastic material obeying a Mooney's constitutive law (Secomb *et al.* 1986). Requiring in particular that the material is linear or neo-Hookean (Li *et al.* 1988), we obtain

$$\tau^{\mathrm{d}} = \frac{\kappa}{2}\left(\lambda_s^2 - \frac{1}{\lambda_s^2}\right), \tag{2.17}$$

where κ is the shear modulus of elasticity. Note that at the initial instant $\tau^{\mathrm{d}} = 0$.

Inserting (2.17) into (2.10), and substituting into (2.16) we obtain a linear integral equation for τ^{m}. Unfortunately, we were not able to theoretically assess the uniqueness of solution of this equation, except in the special case of a cell with isotropic tension and constant mean curvature. In this case τ^{m} may be defined within an arbitrary constant. Physically, this implies that the pressure within the cell may be set to an arbitrary level without any consequences on fluid motion or cell deformation. In any case, solving the derived integral equation allows the computation of the membrane velocity using (2.5).

2.3. *Numerical solution of the integral equation*

In our numerical procedure we trace contour of the cell in a meridional plane with a set marker points, $\boldsymbol{x}_i = (x_i, \sigma_i)$, $i = 1, \ldots, N+1$, as indicated in figure 2. These points are equally spaced with respect to a suitably chosen Lagrangian variable $\beta (0 < \beta < \pi)$. We approximate the cell contour with a set of circular arcs, each passing through trios of successive marker points, associate with each marker point a value of the isotropic tension τ_i^{m}, and compute the derivatives $\mathrm{d}\tau^{\mathrm{m}}/\mathrm{d}s$ by approximating τ^{m} with a fifth-degree polynomial with respect to s in the vicinity of each marker point. Furthermore, we approximate $\Delta \boldsymbol{f}$ with a linear function with respect to arclength between two successive points. This discrete representation allows us to write (2.16) in the symbolic form

$$F(\boldsymbol{x}_0; \{\boldsymbol{x}_i\}, \{\tau_i^{\mathrm{m}}\}) = 0, \tag{2.18}$$

where the function F is identified with the left-hand side of (2.16). To make the linear dependence of F on τ_i^{m} explicit, we rewrite (2.18) in the form

$$C_j(\boldsymbol{x}_0; \{\boldsymbol{x}_i\})\tau_j^{\mathrm{m}} = G(\boldsymbol{x}_0; \{\boldsymbol{x}_i\}), \tag{2.19}$$

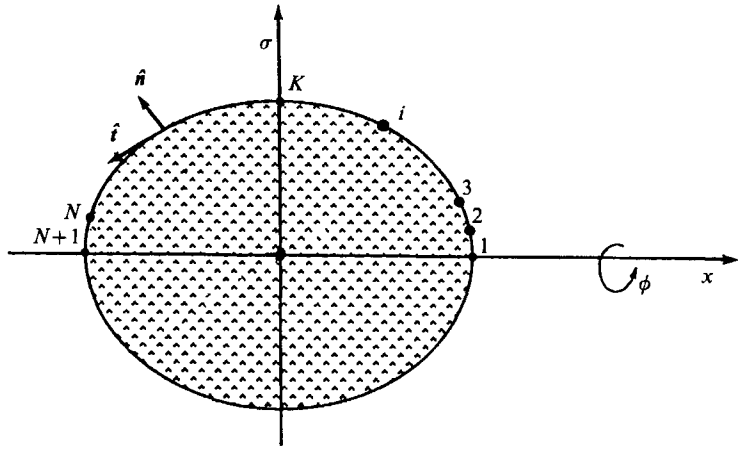

FIGURE 2. Discretization of the cell contour in a meridional plane.

where
$$C_j(\boldsymbol{x}_0;\{\boldsymbol{x}_i\}) \equiv \frac{\partial F}{\partial \tau_j^{\mathrm{m}}}, \tag{2.20a}$$

$$G(\boldsymbol{x}_0;\{\boldsymbol{x}_i\}) \equiv -F(\boldsymbol{x}_0;\{\boldsymbol{x}_i\},\{\tau_i^{\mathrm{m}}=0\}), \tag{2.20b}$$

and the summation convection is implied for the repeated index j in (2.19). In practice, we find convenient to compute $\boldsymbol{C}$ using the difference formula

$$C_j = F(\boldsymbol{x}_0;\{\boldsymbol{x}_i\},\{\tau_i^{\mathrm{m}}=\delta_{ij}\}) - F(\boldsymbol{x}_0;\{\boldsymbol{x}_i\},\{\tau_i^{\mathrm{m}}=0\}). \tag{2.21}$$

When (2.19) is applied at the $N+1$ marker points on the cell surface $\{\boldsymbol{x}_0=\boldsymbol{x}_l, l=1, \ldots, N+1\}$, it provides us with $N+1$ linear algebraic equations for the unknown mean tension τ_i^{m}. Note that (2.19) is trivially satisfied at $i=1$, and thus it must be replaced with its derivative with respect to arclength. To avoid this complication, we express τ_1^{m} with respect to τ_2^{m} and τ_3^{m} using parabolic extrapolation. The size of the resulting linear system may be reduced by exploiting the fore-and-aft symmetry of the cell shape. Thus, we set $\tau_i^{\mathrm{m}}=\tau_{2K-i}^{\mathrm{m}}$, where $K=N/2+1$, and N is taken to be even (figure 2). After implementing these modifications, we end up with a set of $K-1$ unknowns, namely $\tau_i^{\mathrm{m}}, i=2,\ldots,K$ and a system of $K-1$ equations,

$$C_j(\boldsymbol{x}_l;\{\boldsymbol{x}_i\})\,\tau_j^{\mathrm{m}} = G(\boldsymbol{x}_l;\{\boldsymbol{x}_i\}), \quad l=2,\ldots,K, \tag{2.22}$$

which we solve using regular Gauss elimination. Having obtained $\{\tau_i^{\mathrm{m}}\}$, we compute the velocity at the marker points by performing contour integration as required by (2.5). The singular part of the integral is subtracted-off and integrated analytically over each arc (Pozrikidis 1990). Finally, we advance the position of the marker points using simple time stepping (Euler's method). In the majority of our calculations, we maintained the number of points constant throughout a run. In certain instances though, we introduced mechanisms of point removal and addition, as discussed by Pozrikidis (1990).

It is worth noting that we have implemented various modifications of the above procedure, using higher- and lower-order local polynomial approximations for the unknown functions. The above procedure, however, gave most stable and accurate results in the range of parameters considered. We have also implemented an alternative method of solution based on a spectral expansion of the isotropic tension with respect to arclength. The coefficients in the Fourier series were computed by

collocation, that is, by enforcing (2.18) at the marker points. For moderate cell deformations, the spectral method gave results indistinguishable from those obtained by the method described above. For large deformations, the spectral method was less accurate.

All computations were carried out on a SUN-4 computer of our Computational Fluid Mechanics Laboratory. In the majority of our computations we used $K = 48$ or 64. A single time step required approximately 45 s of CPU time. The cell volume changed by less than 0.10 %, while the total surface area changed by less than 0.50 % from the beginning to the end of a calculation. The product of the principal extension ratios $\lambda_s \lambda_\phi$, theoretically equal to 1, remained within 1 ± 0.001 all around the cell contour in all calculations.

2.4. *Numerical smoothing*

During the course of our computations we observed the onset of saw-tooth numerical instabilities with wavelength equal to twice the separation between two successive points. These instabilities first manifested themselves in the distribution of the isotropic membrane tension, and then in the position of the marker points. They disappeared when the number of points was increased to a sufficiently high level and the size of the time step was set to a sufficiently small value. It was suspected that the instabilities were due to the absence of bending resistance, but proving this possibility requires detailed investigations.

To eliminate the observed instabilities, while maintaining the number of points at a moderate level, we decided to smooth out small-scale irregularities in the distribution of the isotropic tension, and in the position of the marker points. Three mechanisms of smoothing were tested. The first mechanism entailed reposition of the marker points on the least-square parabola which is defined by five successive marker points. The second mechanism was based on a Fourier decomposition of the sets $\{x_i, \beta_i\}$ and $\{\sigma_i, \beta_i\}$, where we recall that β is a Lagrangian parameter around the meridional contour. Smoothing was effected by recomputing the position of all marker points using only a portion of the Fourier spectrum. The third mechanism of smoothing was based on the five-point formula proposed by Longuet-Higgins & Cokelet (1976), and successfully used in the computation of breaking water waves. Of the three mechanisms of smoothing, the third one gave most accurate and stable results, and was adopted in the majority of our computations. Best results were obtained when smoothing was applied not only to the position of the marker points, but also to the distribution of the isotropic membrane tension, just before the computation of the velocities.

Saw-tooth instabilities, apparently similar to the ones encountered in our calculations, were also observed by several previous workers including Rallison & Acrivos (1978) for liquid drops, and Li *et al.* (1988) for capsules confined by elastic membranes. The former authors were able to cure the problem by decreasing the size of the time step to a sufficiently low level (see also Pozrikidis 1990). Unfortunately, this is not possible in our case, for our instability is caused not only with the temporal but also with the spatial discretization, requiring small time steps *and* a large number of points. It is this dual requirement that raises pragmatic difficulties, and necessitates numerical smoothing. The instabilities observed by Li *et al.* (1988) are likely to be similar in nature to the ones infesting our calculations. These authors also had to apply numerical smoothing which they effected using cubic splines.

3. A family of stationary cell shapes

It is plausible that when placed in a uniaxial straining flow, a cell will start deforming along its axis of symmetry. Furthermore, it is plausible that after an initial deformation period, the cell might attain a stationary configuration which depends on the unstressed cell shape as well as on the mechanical properties of the bounding membrane. In the case of isotropic membrane tension (vanishing shear elasticity), the asymptotic cell shape might be independent of the unstressed cell shape. This is because the instantaneous membrane tension is independent of the position of elementary particles on the cell membrane relative to their position at the initial instant. It is then natural to consider the shape of stationary configurations with isotropic tension, viewed as asymptotic configurations of cells that have undergone transient deformations.

Our search for stationary cell configurations will be based on the proposition that *spheroidal cells with isotropic tension, axisymmetrically placed in a uniaxial straining flow, constitute stationary configurations*. To demonstrate the validity of this proposition, we shall show that the hydrodynamic surface stress distribution exerted on a stationary spheroidal cell is consistent with the membrane force balance expressed by (2.10). In our analysis, we shall maintain the notation and non-dimensionalization introduced in the preceding sections.

Essential to our analysis is the work of Jeffery (1922) who showed that the surface stress acting on the external surface of an ellipsoidal particle which is immersed in a general linear flow, is given by

$$\boldsymbol{f}_1 = (-P_0 \boldsymbol{I} + \boldsymbol{A}) \cdot \hat{\boldsymbol{n}}. \tag{3.1}$$

Here P_0 is a constant reference pressure, and $\boldsymbol{A}$ is a constant matrix whose elements are functions of the type of flow and of the geometry of the ellipsoid. The remarkably simple form of (3.1) (a constant matrix multiplied by the normal vector) was noted by several previous authors, and was exploited to derive the rheological properties of dilute suspensions of deformable ellipsoids (Cerf 1951; Roscoe 1967; Goddard & Miller 1967). Decomposing $\boldsymbol{f}_1$ into its normal and tangential components we obtain

$$\boldsymbol{f}_1 = (-P_0 + \hat{\boldsymbol{n}} \cdot \boldsymbol{A} \cdot \hat{\boldsymbol{n}}) \hat{\boldsymbol{n}} + \boldsymbol{A} \cdot \hat{\boldsymbol{n}} - (\hat{\boldsymbol{n}} \cdot \boldsymbol{A} \cdot \hat{\boldsymbol{n}}) \hat{\boldsymbol{n}}. \tag{3.2}$$

We concentrate now on a spheroid which is parametrically described by the equations $x = a\cos\beta$, $\sigma = b\sin\beta$, $0 < \beta < \pi$; a is the axis of the spheroid in the x-direction, and b is the axis of the spheroid in the polar σ-direction. For the uniaxial straining flow described by (2.1), $\boldsymbol{A}$ is a diagonal matrix with $A_{22} = A_{33}$. The exact expressions for the diagonal terms, extracted from the work of Jeffery (1922, p. 167), are

$$A_{11} = -2A_{22} = -2A_{33} = \frac{8}{3g_2''}, \tag{3.3a}$$

where

$$g_2'' = \int_0^\infty \frac{u\,\mathrm{d}u}{(E^{\frac{4}{3}}+u)^{\frac{3}{2}}(E^{-\frac{2}{3}}+u)^2}, \tag{3.3b}$$

and E is the aspect ratio of the cell $E = a/b$ (see also Roscoe 1967, §8). Applying (3.2) we find that the surface stress on the external side of the spheroid is given by

$$\boldsymbol{f}_1 = (-P_0 + A_{11}\hat{n}_x^2 + A_{22}\hat{n}_\sigma^2)\hat{\boldsymbol{n}} + (A_{22} - A_{11})\hat{n}_x \hat{n}_\sigma \hat{\boldsymbol{t}}. \tag{3.4}$$

We recall now that the spheroid represents a stationary cell whose internal velocity

vanishes, and whose internal pressure is a constant, call it $P_{\rm Int}$. The surface stress on the internal side of the cell is thus equal to

$$\boldsymbol{f}_2 = -P_{\rm Int}\,\hat{\boldsymbol{n}}. \tag{3.5}$$

Subtracting the last two equations we obtain

$$\Delta\boldsymbol{f} \equiv \boldsymbol{f}_1 - \boldsymbol{f}_2 = (P_{\rm Int} - P_0 + A_{11}\,\hat{n}_x^2 + A_{22}\,\hat{n}_\sigma^2)\,\hat{\boldsymbol{n}} + (A_{22} - A_{11})\,\hat{n}_x\,\hat{n}_\sigma\,\hat{\boldsymbol{t}}. \tag{3.6}$$

We now inquire whether this expression is consistent with the membrane force balance expressed by (2.10) with $\tau^{\rm d} = 0$. Specifically, we ask whether there exists a function $\tau^{\rm m}$, identified with the isotropic membrane tension, such that both of the following equations are satisfied:

$$(k_s + k_\phi)\,\tau^{\rm m} = P_{\rm Int} - P_0 + A_{11}\,\hat{n}_x^2 + A_{22}\,\hat{n}_\sigma^2, \tag{3.7a}$$

$$\frac{{\rm d}\tau^{\rm m}}{{\rm d}s} = (A_{11} - A_{22})\,\hat{n}_x\,\hat{n}_\sigma. \tag{3.7b}$$

We note that for a spheroid

$$k_s + k_\phi = \frac{E}{b}\frac{1 + \cos^2\beta + E^2\sin^2\beta}{(E^2\sin^2\beta + \cos^2\beta)^{\frac{3}{2}}}, \tag{3.8a}$$

$$\hat{n}_x = \frac{\cos\beta}{(E^2\sin^2\beta + \cos^2\beta)^{\frac{1}{2}}}, \quad \hat{n}_\sigma = \frac{E\sin\beta}{(E^2\sin^2\beta + \cos^2\beta)^{\frac{1}{2}}}. \tag{3.8b}$$

Substituting (3.8a, b) into (3.7a) and solving for $\tau^{\rm m}$ we obtain

$$\tau^{\rm m} = \frac{b}{E}\frac{(P_{\rm Int} - P_0 + A_{22})E^2\sin^2\beta + (P_{\rm Int} - P_0 + A_{11})\cos^2\beta}{(E^2+1)\sin^2\beta + 2\cos^2\beta}E^2\sin^2\beta + \cos^2\beta. \tag{3.9}$$

On the other hand, using (3.8b) we rewrite (3.7b) in the equivalent form

$$\frac{{\rm d}\tau^{\rm m}}{{\rm d}s} = a\frac{A_{11} - A_{22}}{E^2 - 1}\frac{\rm d}{{\rm d}s}(E^2\sin^2\beta + \cos^2\beta)^{\frac{1}{2}}, \tag{3.10}$$

which upon integration yields

$$\tau^{\rm m} = a\frac{A_{11} - A_{22}}{E^2 - 1}(E^2\sin^2\beta + \cos^2\beta)^{\frac{1}{2}} + D, \tag{3.11}$$

where D is an arbitrary constant. We then arrive at the rather remarkable conclusion that (3.9) and (3.11) are identical provided that

$$2(P_{\rm Int} - P_0 + A_{22})E^2 = (E^2+1)(P_{\rm Int} - P_0 + A_{11}), \tag{3.12a}$$

$$D = 0. \tag{3.12b}$$

With the aid of (3.3a), the first of these conditions gives

$$P_{\rm Int} - P_0 = \frac{8}{3g_2''}\frac{2E^2+1}{E^2-1}. \tag{3.13}$$

This equation relates the pressure inside the cell to that at infinity. Note that as the spheroid tends to obtain a spherical shape, $E \to 1$, $P_{\rm Int}$ increases without limit. The pressure difference $\Delta P = P_{\rm Int} - P_0$ is positive for prolate shapes ($E > 1$), and negative for oblate shapes ($E < 1$). In figure 3(a) we plot $P_{\rm Int} - P_0$ as a function of the aspect

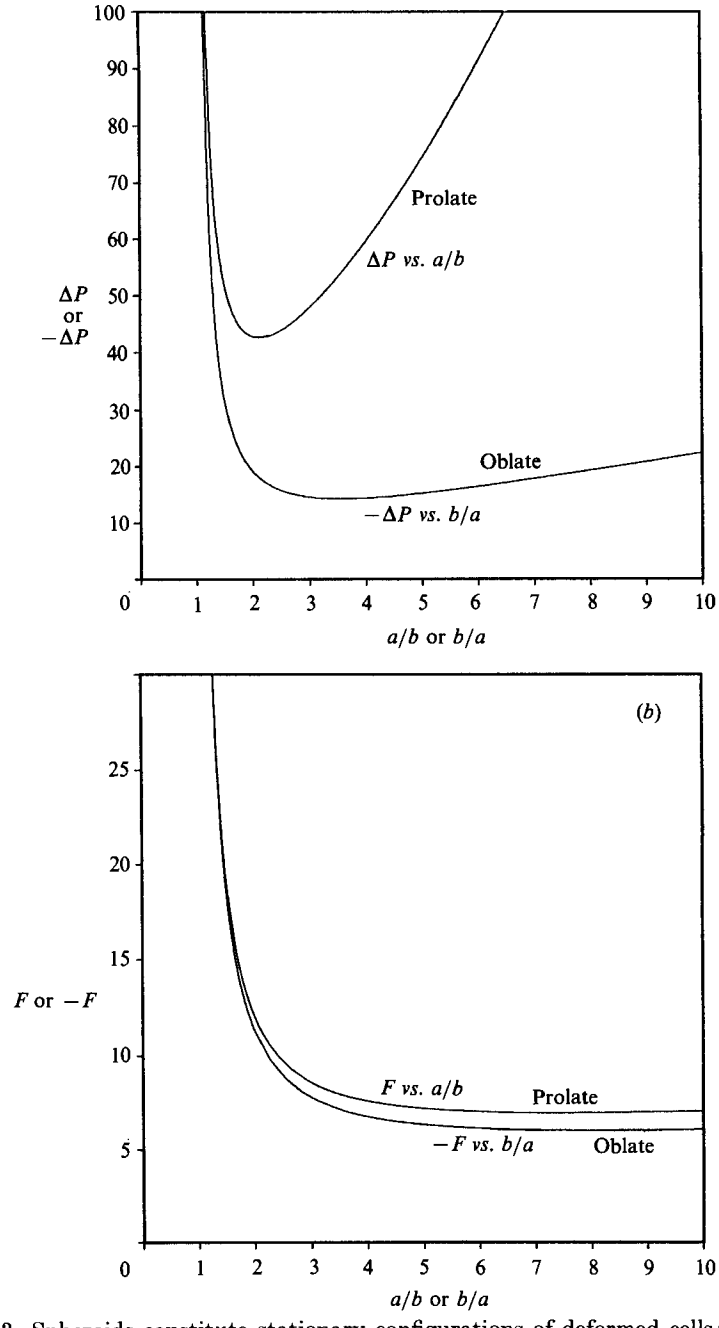

FIGURE 3. Spheroids constitute stationary configurations of deformed cells: (*a*) the internal cell pressure $\Delta P = P_{\text{Int}} - P_0$, and (*b*) the amplitude of the isotropic membrane tension $F \equiv 4ag_2''/(E^2-1)$, plotted with respect to the spheroid aspect ratio a/b or b/a, for prolate and oblate shapes.

ratio $E = a/b$ for prolate shapes, and $P_0 - P_{\text{Int}}$ as a function of $1/E = b/a$ for oblate shapes. We observe that as a prolate spheroid becomes increasingly more eccentric, $P_{\text{Int}} - P_0$ decreases, reaches a minimum at $a/b = 2.13$, and then starts increasing. Similarly, as an oblate cell obtains a more disk-like shape, the internal pressure increases, reaches a maximum at $b/a = 3.57$, and then starts decreasing.

Using (3.11) and (3.3a), we find that the distribution of the membrane tension is given by

$$\tau^{\mathrm{m}} = F(E^2 \sin^2\beta + \cos^2\beta)^{\frac{1}{2}}, \tag{3.14a}$$

where

$$F \equiv \frac{4ag_2''}{E^2-1}. \tag{3.14b}$$

The membrane tension is positive for prolate shapes $E > 0$ (the membrane is stretched), and negative for oblate shapes $E < 0$ (the membrane is compressed). As the spheroid tends to become a sphere, $E \to 1$, the membrane tension increases in magnitude without limit. This behaviour is also evident in figure 3(b) where we plot the amplitude of the distribution F versus the aspect ratio $E = a/b$ or $1/E = b/a$. For prolate shapes, as a/b is increased, F decreases, reaches a weak minimum, and then starts increasing. It is interesting to note that beyond $a/b = 4$, the membrane tension is virtually insensitive to the aspect ratio. Within the range of figure 3(b), minimum F corresponds to $E = a/b = 8.0$. Similarly, as the spheroid obtains a disk-like shape, that is, as $1/E = b/a$ is increased, the magnitude of F decreases, reaches a weak minimum at $b/a = 7.5$, and then starts increasing.

The above results clearly indicate that the spherical shape constitutes a singular case for it is associated with infinite values for the internal pressure and for the membrane tension. Physically, this may be attributed to the fact that a spherical cell may not deform under constant volume without increasing its surface area.

The analysis in this section may be conveniently used to test the validity and accuracy of the numerical procedure for transient deformations described in the preceding section. Our computations confirmed that, indeed, prolate and oblate spheroidal cells with isotropic tension constitute stationary configurations. As will be seen in the next section, the computed stationary membrane tensions were in perfect agreement with those predicted by (3.14a, b). In addition, our results showed that prolate shapes are stable, whereas oblate shapes are unstable to axisymmetric perturbations in shape. Indeed, in our computations, perfectly oblate spheroids survived for a limited time, and then they developed small-scale irregularities initiated by numerical error. Perturbed oblate spheroids deformed into corresponding prolate spheroids with same volume and surface area, as will be described in the next section.

4. Transient cell deformations

In this section we investigate transient cell deformations maintaining the non-dimensionalization of the preceding sections. It will be convenient to introduce two new dimensionless parameters: the membrane modulus of elasticity $k = \kappa/\mu e a$, and the sphericity index $\mathscr{S}$,

$$\mathscr{S} = \frac{(A/4\pi)^{\frac{1}{2}}}{(3V/4\pi)^{\frac{1}{3}}}. \tag{4.1}$$

A is the total surface area, and V is the volume of a cell, and both are conserved during a transient cell deformation. For the sphere $\mathscr{S} = 1$, while for any other shape $\mathscr{S} > 1$. Note that under the adopted non-dimensionalization, constant $\mathscr{S}$ implies constant surface area. For prolate spheroidal cells, the sphericity index is related to the aspect ratio $E = a/b$ through the relationship

$$\mathscr{S} = \frac{1}{\sqrt{2}E^{\frac{1}{3}}}\left[1 + \frac{E^2}{(E^2-1)^{\frac{1}{2}}}\arcsin\frac{(E^2-1)^{\frac{1}{2}}}{E^2}\right]^{\frac{1}{2}}. \tag{4.2}$$

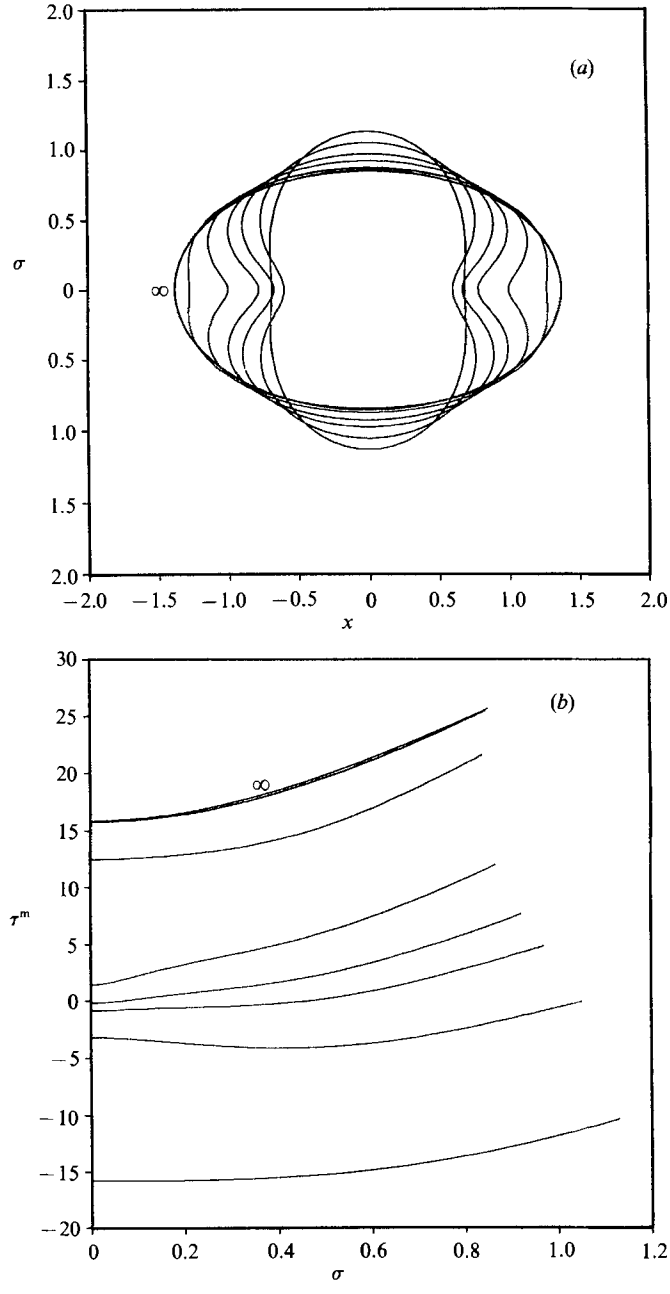

FIGURE 4. (*a*) Characteristic stages in the deformation of an oblate cell with $\epsilon = -0.300$, and $k = 0$, at times 0, 0.0975, 0.1725, 0.2250, 0.3000, 0.3750, 0.5025; the shape labelled ∞, which is indistinguishable from that at time 0.5025, is a perfect spheroid with the same volume and surface areas as the original cell; (*b*) the isotropic tension distribution for the deformation stages shown in (*a*).

In the main body of our computations we consider cells whose unstressed shape is described by

$$r = \delta(1 + \epsilon P_2(\cos\theta)) \tag{4.3}$$

where P_2 is the second-degree Legendre polynomial, ϵ is an arbitrary constant which

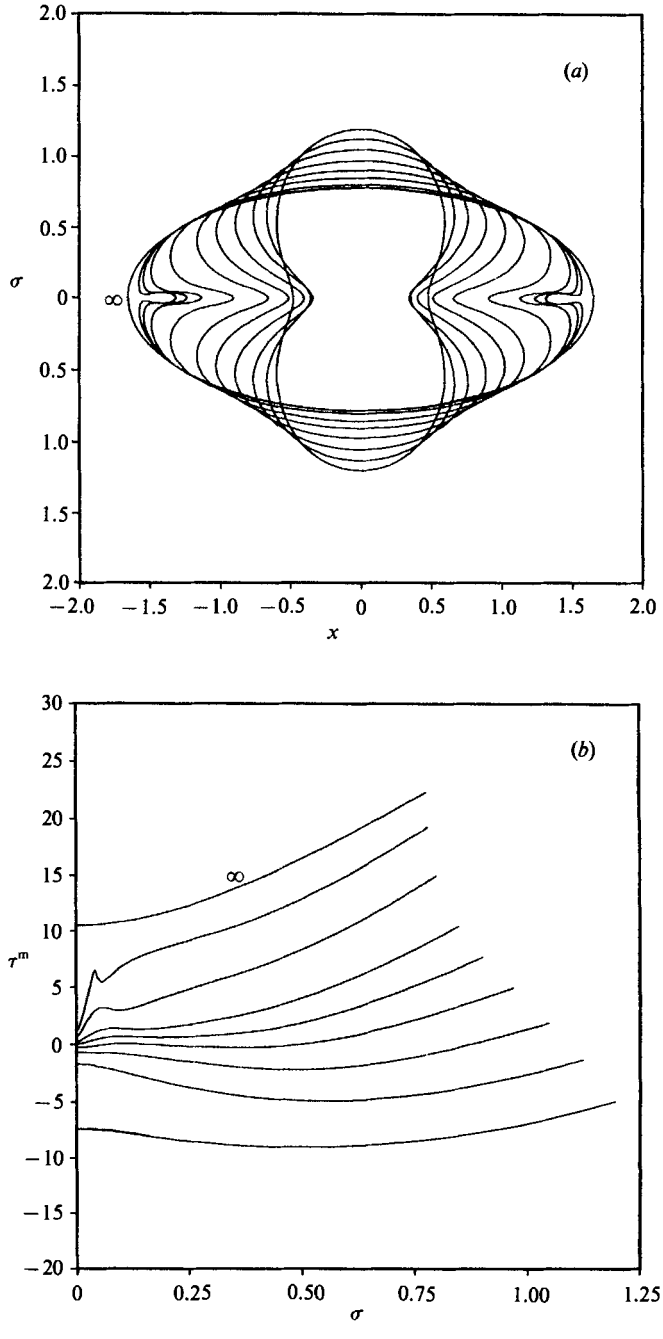

FIGURE 5. (*a*) Characteristic stages in the deformation of an oblate cell with $\epsilon = -0.500$, and $k = 0$, at times 0, 0.0825, 0.1500, 0.2250, 0.3000, 0.3750, 0.4800, 0.5700, 0.6150, 0.6525; the shape labelled ∞ is a perfect spheroid with the same volume and surface area as the original cell; (*b*) the isotropic tension distribution for the first eight stages shown in (*a*).

varies between -1 and 2, and θ is the polar angle in a meridional plane (figure 1). The scaling constant δ is a function of ϵ and is chosen such that the cell volume is equal to $4\pi/3$. Positive ϵ produces prolate shapes, while negative ϵ gives oblate shapes. The oblate shapes produced by (4.3) resemble spheroids or biconcave disks and thus they provide us with convenient prototypes for studying the stability of spheroidal cells and the deformation of red blood cells.

First, we consider oblate cells with negative values of ϵ, and with isotropic membrane tension, $k = 0$. In figure 4(*a*) we present characteristic stages in the evolution of a cell with $\epsilon = -0.300$, and corresponding sphericity index $\mathscr{S} = 1.0168$. We observe that at small times, the cell is squeezed along the x-axis under the action of the imposed straining flow. A portion of the cell membrane close to the axis of symmetry starts moving towards the midplane of the cell, causing the formation of an axisymmetric dimple. At $t = 0.1725$, the dimple has attained maximum size. At latter times, the main body of the cell continues being elongated along the x-axis, and the dimple begins to shrink. Asymptotically at large times, the cell reduces into a spheroid with aspect ratio $a/b = 1.616$ or $\mathscr{S} = 1.0188$, labelled ∞ in figure 4(*a*). Thus, our numerical results support the idea that the cell deforms into a stationary ellipsoid. In figure 4(*b*) we plot the distribution of the isotropic membrane tension for the evolution stages illustrated in figure 4(*a*). The membrane tension is initially negative, but becomes positive when the cell has been sufficiently elongated along the x-axis. We shall comment on the significance of negative tension in the next section. Overall, the transition from the initial to the final tension distribution proceeds in a smooth fashion.

In figure 5(*a*) we present characteristic stages in the evolution of a cell with $\epsilon = -0.500$, and $\mathscr{S} = 1.044$. The initial stages of deformation are similar to those described in figure 4(*a*) for $\epsilon = -0.30$. We note, however, that as the cell is elongated along the x-axis, the dimple transforms into a persistent depression at the tip of the cell. At large times, the main body of the cell closes upon itself along the x-axis, and the cell reduces into a spheroid that contains two small pockets at either tip. The label ∞ in figure 5(*a*) indicates a spheroidal cell with volume and surface area identical to those of the original undeformed cell. Although calculations at large times were prohibited by the onset of severe irregularities in the distribution of the membrane tension, the results indicate that the main portion of the cell does attain a spheroidal shape. In figure 5(*b*) we plot the distribution of the membrane tension for the various stages shown in figure 5(*a*). The tension is compressive at small times, and stretching at large times. Asymptotically at large times, the distribution of tension over the main body of the cell tends to that for a spheroid. The irregular behaviour around the tip of the spheroid is indicative of membrane folding. As mentioned above, the details of the membrane tension distribution at the final stages of deformation could not be resolved with acceptable accuracy in our computations.

We now turn to investigate the effect of shear elasticity, expressed by the dimensionless parameter k. In figure 6(*a*, *b*) we present two sequences of cell profiles for $\epsilon = -0.30$, and $k = 10$, and 20. Figure 6(*a*), corresponding to $k = 10$, suggests that increasing the shear elasticity reduces the size of the dimple, but causes the formation of a transient region of small curvature at the base of the dimple. At large times, the cell reduces into an almost perfect spheroid. For the purposes of comparison, in figure 6(*a*), and under the label ∞, we have drawn a perfect spheroid with the same volume and surface area as the initial cell. Comparing the times for the various evolution stages shown in figure 6(*a*) and figure 4(*a*) we find that as k is

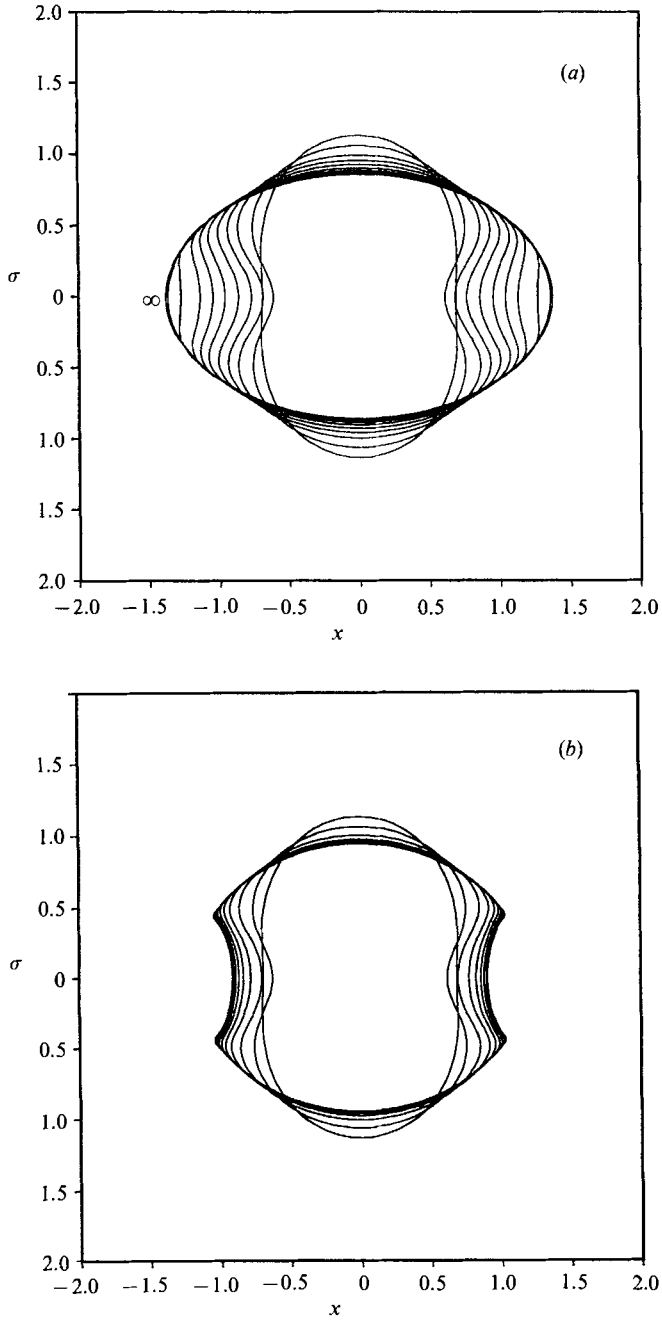

FIGURE 6. The effect of shear elasticity: characteristic stages in the deformation of an oblate cell with $\epsilon = -0.300$, and (*a*) $k = 10$ at times 0, 0.0950, 0.1750, 0.2350, 0.3000, 0.3750, 0.4500, 0.5400, 0.7000, 0.98500; the shape labelled ∞ is a perfect spheroid with the same volume and surface area as the original cell; (*b*) $k = 20$ at times 0, 0.10, 0.20, 0.30, 0.4025, 0.5025, 0.6025, 0.7025, 0.8025, 0.8825.

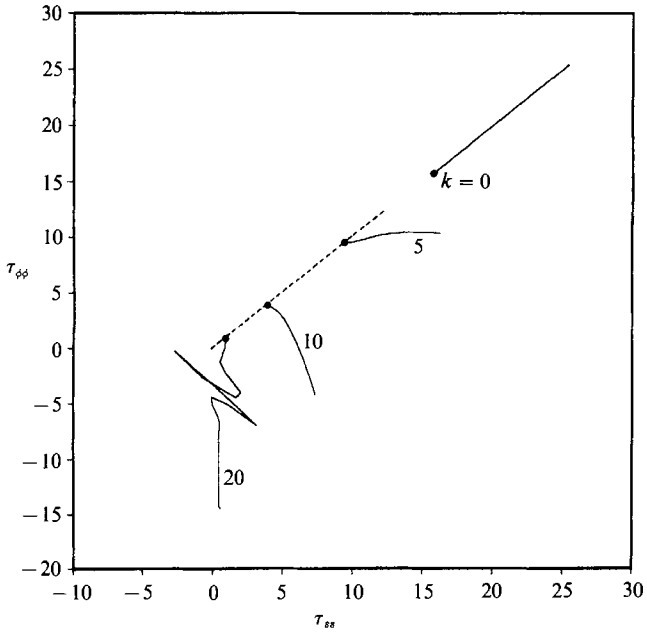

FIGURE 7. The effect of shear elasticity: a plot of the azimuthal versus the meridional membrane tension along the cell contour, at an asymptotic stage of evolution, for $\epsilon = -0.300$, and $k = 0, 5, 10, 20$. The tip of the spheroid is indicated with a dot. Note that for $k = 0$, or along the axis of deformation, these tensions are equal.

increased, the rate of cell deformation is reduced. Turning to figure 6(*b*), corresponding to $k = 20$, we observe a drastic change in behaviour; the cell deforms into a stationary compound shape which is composed of a main spheroidal body and of two large concave regions at either tip. The radius of curvature of the membrane at the base of each concave region is monotonically decreasing in time, indicating the spontaneous appearance of a sharp corner. Unfortunately, because of the necessary numerical smoothing, we were not able to resolve with confidence the asymptotic behaviour of the radius of curvature at the corner. One has to keep in mind however, that however small the bending resistance, bending stresses become important in the vicinity of sharp corners because of the large local curvature, and hence our simplified model is bound to be of limited accuracy.

Proceeding, we consider the effect of shear elasticity on the magnitude of the developing membrane tensions. Thus, in figure 7 we plot the azimuthal membrane tension $\tau_{\phi\phi}$ against the meridional membrane tension τ_{ss} along the cell contour, at the asymptotic stages of deformation (the dots indicate the tip of the cell). These tensions are identical when $k = 0$, for the cell membrane tension is isotropic. Overall, we observe that increasing k causes a decrease in the magnitude of both τ_{ss} and $\tau_{\phi\phi}$. For $k = 0, 5, 10$, the azimuthal tension is always smaller than the meridional one, as suggested by the fact that all curves in figure 7 lie on or below the diagonal line. For $k = 10$, $\tau_{\phi\phi}$ becomes negative over a substantial portion of the cell contour. The physical significance of this behaviour will be discussed in the next section. For $k = 20$, we observe an irregular behaviour, indicative of the formation of a sharp corner. Over the central portion of the membrane τ_{ss} is nearly constant, close to zero, whereas $\tau_{\phi\phi}$ shows rapid variations.

When viewed in comparison with figure 5(*a*), the results of figure 6(*a*, *b*) strongly

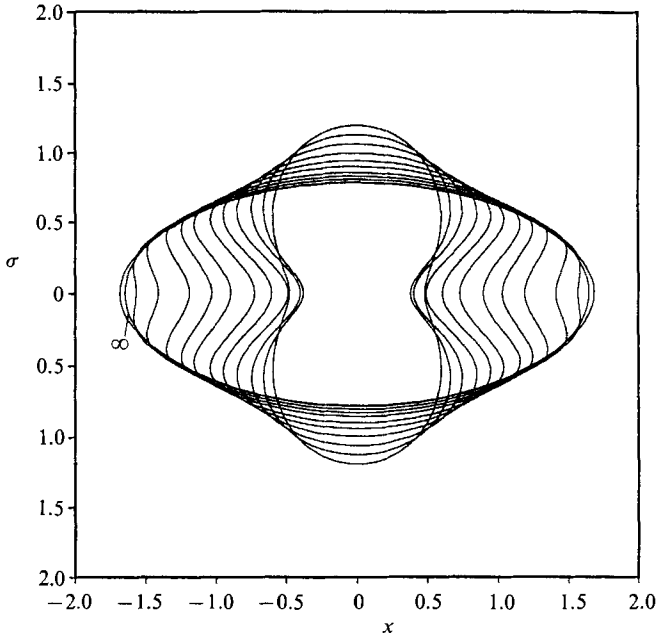

FIGURE 8. The effect of shear elasticity: characteristic stages in the deformation of an oblate cell with $\epsilon = -0.500$, and $k = 5$, at times 0, 0.0825, 0.150, 0.2250, 0.3000, 0.3750, 0.4800, 0.5700, 0.68250, 0.8475, 0.9750, 0.1775; the shape labelled ∞ is a perfect spheroid with the same volume and surface area as the original cell.

suggest that shear elasticity prevents membrane folding. This is indeed verified by the results presented in figure 8, depicted the evolution of a cell with $\epsilon = -0.50$, and $k = 5$. In this case, despite the pronounced initial disk-like shape, no folding occurs during the cell evolution.

We now turn our attention to prolate shapes, with positive values of ϵ. Admittedly, the physical significance of these shapes is weaker than that for oblate shapes, but their study is of some academic value. In figure 9(*a*) we present successive stages in the evolution of an initially prolate cell with $\epsilon = 0.50$, sphericity index $\mathscr{S} = 1.038$, and isotropic membrane tension $k = 0$. Note that the unstressed shape, at $t = 0$, contains a slight axisymmetric dimple at the midplane $x = 0$. As the cell is stretched under the action of the imposed elongational flow, the depth of this dimple decreases. Asymptotically at large times, the cell transforms into a perfect spheroid with aspect ratio $E = a/b = 2.014$, labelled $t = \infty$. In figure 9(*b*) we present the distribution of the membrane tension for the various profiles presented in figure 9(*a*). As the cell starts deforming, the magnitude of the membrane tension increases all around the contour of the cell. At large times, the distribution of the membrane tension reduces to that for the prolate spheroid. This transition is not monotonic, but proceeds through an overshooting at the final stages of deformation.

The evolution of prolate cells with different values of ϵ is similar to that described in figure 9(*a*, *b*). As an example, in figure 10(*a*) we present characteristic stages in the evolution of a cell with $\epsilon = 1.00$, $k = 0$. Asymptotically at large times, the cell reduces into a perfect prolate spheroid with $E = 3.118$. Figure 10(*b*) shows the corresponding transient distributions of the isotropic membrane tension. There is an overshooting of the membrane distribution at the final stages of deformation, similar to that observed in figure 9(*b*). The membrane tension is positive at all times.

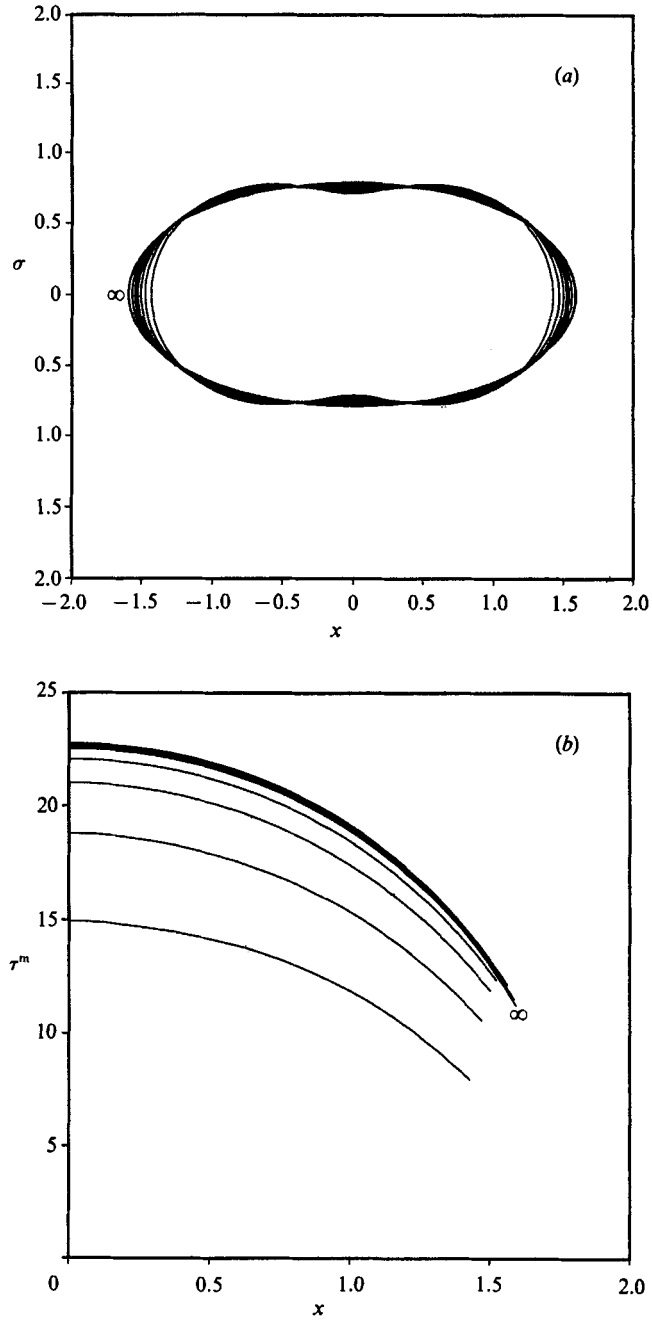

FIGURE 9. (*a*) Characteristic stages in the deformation of a prolate cell with $\epsilon = 0.500$, and $k = 0$, at times 0, 0.250, 0.500, 0.7650, 0.100, 0.1500, 0.290; the shape labelled ∞, which is indistinguishable from that at time 0.2900, is a perfect spheroid with the same volume and surface area as the original cell; (*b*) the isotropic tension distribution for the stages shown in (*a*); note the overshooting of the distribution at the final stages of deformation.

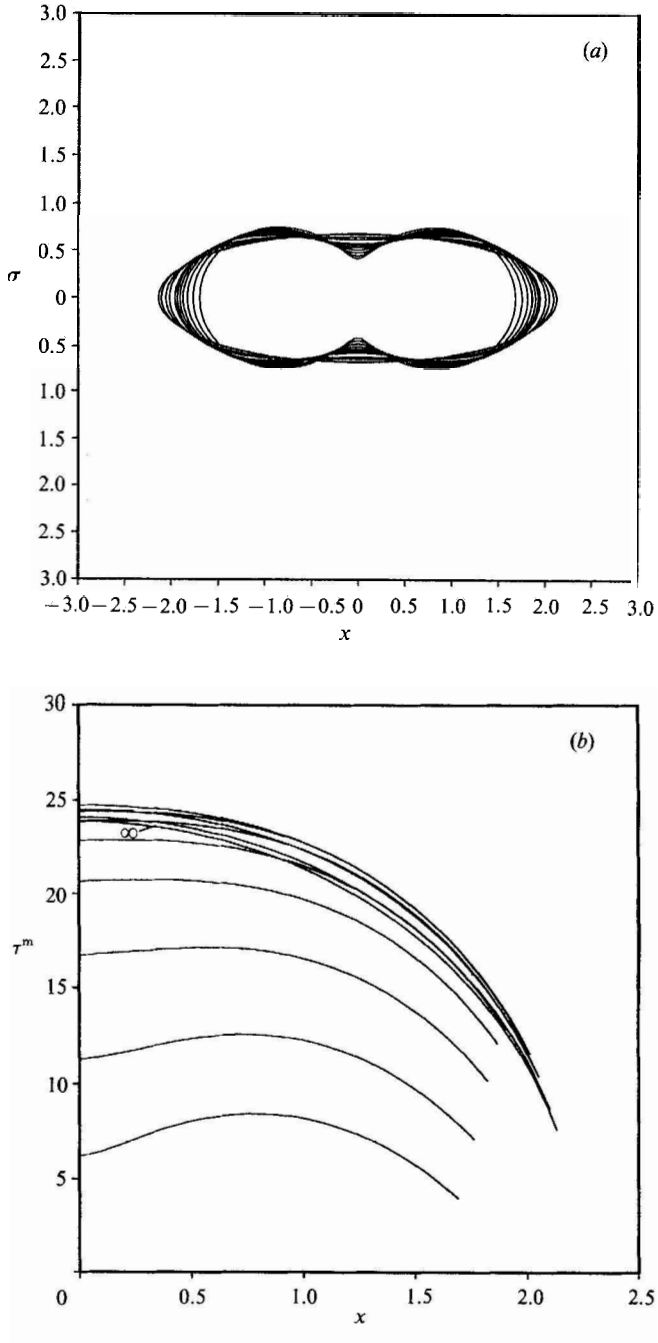

FIGURE 10. (*a*) Characteristic stages in the deformation of a prolate cell with $\epsilon = 1.000$, and $k = 0$, at times 0, 0.025, 0.075, 0.1000, 0.2550, 0.3675, 0.6825; the shape labelled ∞, which is indistinguishable from that at time 0.6825, is a perfect spheroid with the same volume and surface area as the original cell; (*b*) the isotropic stress distribution for the stages shown in (*a*); note the overshooting of the tension in the final stages of deformation.

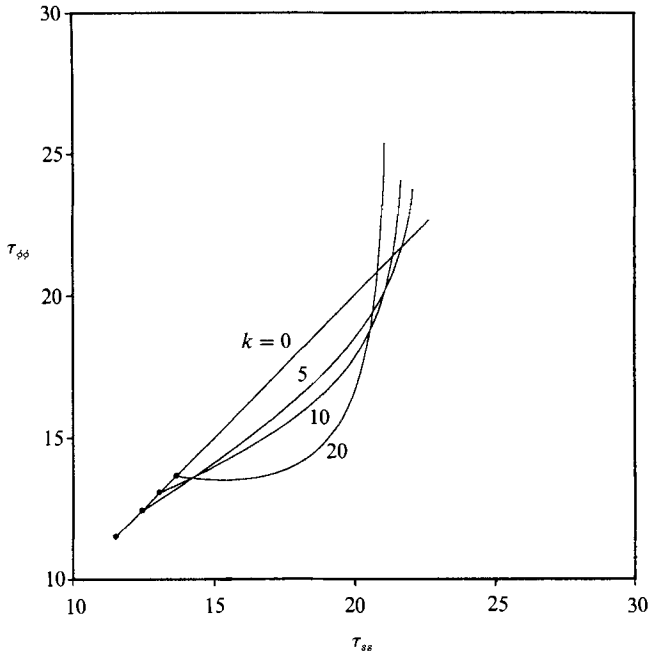

FIGURE 11. The effect of shear elasticity: the azimuthal versus the meridional membrane tension along the cell contour, at the asymptotic stages of evolution, for $\epsilon = 0.5000$, and $k = 0, 5, 10, 20$. The tip of the spheroid is indicated with a dot. Note that for $k = 0$ or along the axis of the cell, these stresses are equal.

For cells with a prolate unstressed shape, the membrane shear elasticity k has only a minor effect on the asymptotic cell configuration, but has a pronounced effect on the magnitude of the transient and asymptotic membrane tensions. To demonstrate this feature, in figure 11 we plot $\tau_{\phi\phi}$ versus τ_{ss} for $\epsilon = 0.50$, and $k = 0, 5, 10, 20$ (a dot indicates the tip of the cell). For finite values of k, near the tip of the cell, τ_{ss} is greater than $\tau_{\phi\phi}$, while near the midplane of the cell, τ_{ss} is smaller than $\tau_{\phi\phi}$. Overall, the magnitude of the membrane stresses does not show appreciable variations with k.

We performed additional calculations using as an initial cell shape the normal shape proposed by Evans & Fung (1972). The results were in qualitative agreement with those described for oblate cells (see in particular figures 5 and 8).

5. Closing remarks

Our calculations showed that when placed in axisymmetric straining flow, prolate or oblate axisymmetric cells with isotropic membrane tension reduce into prolate spheroids. Highly oblate cells may fold and develop a pocket along the axis of deformation. Finite membrane shear elasticity prevents membrane folding, but may catalyse the formation of sharp corners and concave regions along the cell contour. For oblate cells, decreasing the shear elasticity causes an appreciable increase in the magnitude of the developing membrane tensions.

Our analysis for stationary spheroidal cells may be used to obtain an approximate estimate of the maximum strain rate above which a red blood cell is expected to break up. Indeed, it is well established that the average area of a red cell is approximately 44% larger than the minimum area required for the spherical shape

(Skalak *et al.* 1989). Using (4.1) we find that the corresponding sphericity index is equal to 1.20. Furthermore, using (4.2) we find that the eccentricity of a spheroid with volume and surface area identical to those of the cell is $a/b = 6.0$. Equations (3.14a,b) then show that the maximum isotropic tension on this spheroidal cell is approximately equal to 36. Reverting to dimensional variables, and setting the maximum allowable membrane tension to 10 dyn/s (Evans, Waugh & Melnik 1976), we find a maximum permissible rate of strain equal to $e_{\max} = 10/(36\,\mu a)$ (dyn/cm). Using $\mu = 12$ cP (for plasma) and $a = 2.8$ μm (Skalak *et al.* 1989) yields $e_{\max} = 8250\ \mathrm{s}^{-1}$. Since this is only an approximate estimate, we may set $e_{\max} = 10^5\ \mathrm{s}^{-1}$. For comparison, we note that the strain rate usually used in experimental studies of red cells is of the order $10^2\ \mathrm{s}^{-1}$ (Tran-Son-Tay *et al.* 1984).

Our theoretical results for oblate spheroids showed that the membrane tension takes negative values, which means that it is compressive. Similarly, our numerical results showed that in the case of vanishing elasticity, the transient isotropic membrane tension may take negative values. Furthermore, in the case of finite elasticity, not only the transient but also the asymptotic membrane tension may be compressive. This would not seem to be realistic since a cell membrane with zero bending rigidity would immediately buckle under compression. In the numerical solution such a buckling is eliminated by the use of numerical smoothing which appears to give the membrane an artificial finite non-zero bending rigidity. Thus, some of the numerical shapes obtained while representing solutions to the posed problem are unstable solutions and would not be realized in practice. It would then seem imperative to incorporate the bending resistance in the mechanical model for the cell membrane, at the expense, however, of simplicity of modelling and computer programming.

Our results revealed a number of novel mechanisms in the cell deformation whose physical interpretation should be treated with caution. In a large-scale blood flow, red blood cells are instantaneously subjected to three-dimensional elongational and rotational flow fields. Crudely speaking, the elongational component causes cell deformation, while the rotational component causes cell rotation and membrane tank-treading motion. It is likely that the tank-treading motion will inhibit the development of sharp corners and the formation of concave regions along the cell contour. Indeed, observations of red blood cells in a two-dimensional shear flow reveal that the cells deform into elongated ellipsoids with the flat side normal to the plane of flow (Tran-Son-Tay *et al.* 1984).

Comparing our results to those for liquid drops or for capsules confined by elastic membranes, we find an important variation (Rallison & Acrivos 1978; Li *et al.* 1988). When placed in a sufficiently strong elongational flow, both of these particles undergo continuous deformation followed by eventual breakup. In contrast, red cells always undergo finite deformation reducing into spheroids. Thus, the mechanism of destruction of red cells appears to be fundamentally different to that of drops or capsules, as it is exclusively due to the mechanical failure of the enclosing membrane.

Acknowledgment is made to the donors of the Petroleum Research Fund, administered by the American Chemical Society, for partial support of this research. This work is partially supported by the National Science Foundation, Program of Fluid Dynamics and Hydraulics, Grant MSM 88-20350. Discussions with Professor R. Skalak were most helpful. Gratitude is due to the referees of the *Journal of Fluid Mechanics* for their perceptive criticism and invaluable comments.

Appendix

The elements of the matrix $\boldsymbol{M}$ of equation (2.5) are defined as

$$M_{xx} = 2k\left(\frac{\sigma}{\sigma_0}\right)^{\frac{1}{2}}\left(F+\frac{\hat{x}^2}{r^2}E\right),$$

$$M_{x\sigma} = k\frac{\hat{x}}{(\sigma_0\sigma)^{\frac{1}{2}}}\left[F-(\sigma_0^2-\sigma^2+\hat{x}^2)\frac{E}{r^2}\right],$$

$$M_{\sigma x} = -k\frac{\hat{x}}{\sigma_0}\left(\frac{\sigma}{\sigma_0}\right)^{\frac{1}{2}}\left[F+(\sigma_0^2-\sigma^2-\hat{x}^2)\frac{E}{r^2}\right],$$

$$M_{\sigma\sigma} = \frac{k}{\sigma_0\sigma}\left(\frac{\sigma}{\sigma_0}\right)^{\frac{1}{2}}\left[(\sigma_0^2+\sigma^2+2\hat{x}^2)F-(2\hat{x}^4+3\hat{x}^2(\sigma_0^2+\sigma^2)+(\sigma_0^2-\sigma^2)^2)\frac{E}{r^2}\right],$$

where $\hat{x} = x-x_0$, and $$k^2 = \frac{4\sigma\sigma_0}{\hat{x}^2+(\sigma+\sigma_0)^2}.$$

F and E are the complete elliptic integrals of the first and second kind with argument k.

REFERENCES

BARTHES-BIESEL, D. 1980 Motion of a spherical microcapsule freely suspended in a linear shear flow. *J. Fluid Mech.* **100**, 831–853.

BARTHES-BIESEL, D. & RALLISON, J. M. 1981 The time-dependent deformation of a capsule freely suspended in a linear shear flow. *J. Fluid Mech.* **113**, 251–267.

BRUNN, P. O. 1983 The deformation of a viscous particle surrounded by an elastic shell in a general time-dependent linear flow field. *J. Fluid Mech.* **126**, 533–544.

CERF, R. 1951 Recherches theoriques et experimentales sur l'effet Maxwell des solutions de macromolécules déformables I. Théorie de l'effet Maxwell des suspensions de sphères élastiques. *J. Chim. Phys.* **48**, 59–84.

EVANS, E. A. & FUNG, Y. C. 1972 Improved measurements of the erythrocyte geometry. *Microvasc. Res.* **4**, 335.

EVANS, E. A., WAUGH, R. & MELNIK, L. 1976 Elastic area compressibility modulus of red cell membrane. *Biophys. J.* **16**, 585–595.

EVANS, E. A. & SKALAK, R. 1980 *Mechanics and Thermodynamics of Biomembranes.* CRC Press.

FISCHER, T. M. 1989 Mechanical hemolysis of cross-bonded red cells in the microcirculation. *Intl J. Microcirculation: Clin. Exp.* **8**, 159–176.

FUNG, Y. C. 1981 *Biomechanics.* Springer,

GODDARD, J. D. & MILLER, C. 1967 Nonlinear effects in the rheology of dilute suspensions. *J. Fluid Mech.* **28**, 657–673.

JEFFERY, G. B. 1922 The motion of ellipsoidal particles immersed in a viscous fluid. *Proc. R. Soc. Lond.* A **102**, 161–179.

KELLER, S. R. & SKALAK, R. 1982 Motion of a tank-treading ellipsoidal particle in a shear flow. *J. Fluid Mech.* **120**, 27–47.

LI, Z. Z., BARTHES-BIESEL, D. & HELMY, A. 1988 Large deformations and burst of a capsule freely suspended in an elongational flow. *J. Fluid Mech.* **187**, 179–196.

LONGUET-HIGGINS, M. S. & COKELET, E. D. 1976 The deformation of steep surface waves on water I. A numerical method of computation. *Proc. R. Soc. Lond.* A **350**, 1–26.

NIIMI, H. & SUGIHARA, M. 1985 Cyclic loading on the red cell membrane in a shear flow: A possible cause of hemolysis. *J. Biomech. Engng* **107**, 91–95.

POZRIKIDIS, C. 1990 The instability of moving viscous drops. *J. Fluid Mech.* **210**, 1–21.

RALLISON, J. M. & ACRIVOS, A. 1978 A numerical study of the deformation and burst of a viscous drop in an extensional flow. *J. Fluid Mech.* **89**, 191–200.

ROSCOE, R. 1967 On the rheology of a suspension of viscoelastic spheres in a viscous liquid. *J. Fluid Mech.* **28**, 273–293.

SECOMB, T. W., SKALAK, R., OZKAYA, N. & GROSS, J. F. 1986 Flow of axisymmetric red blood cells in narrow capillaries. *J. Fluid Mech.* **163**, 405–423.

SKALAK, R., OSKAYA, N. & SKALAK, T. C. 1989 Biofluid mechanics. *Ann. Rev. Fluid Mech.* **21**, 167–204.

TRAN-SON-TAY, R., SUTERA, S. P. & RAO, P. R. 1984 Determination of red blood cell membrane viscosity from rheoscopic observations of tank-treading motion. *J. Biophys. Soc.* **46**, 65–72.

ZAHALAK, G. I., RAO, P. R. & SUTERA, S. 1987 Large deformations of a cylindrical liquid-filled membrane by a viscous shear flow. *J. Fluid Mech.* **179**, 283–305.